High transport current superconductivity in powder-in-tube Ba$_{0.6}$K$_{0.4}$Fe$_2$As$_2$ tapes at 27T

He Huang[1,2] ⬤, Chao Yao[1], Chiheng Dong[1], Xianping Zhang[1], Dongliang Wang[1], Zhe Cheng[1,2], Jianqi Li[3], Satoshi Awaji[4], Haihu Wen[5] and Yanwei Ma[1,2]

[1] Key Laboratory of Applied Superconductivity, Institute of Electrical Engineering, Chinese Academy of Sciences, Beijing 100190, People's Republic of China
[2] University of Chinese Academy of Sciences, Beijing 100049, People's Republic of China
[3] Beijing National Laboratory for Condensed Matter Physics, Institute of Physics, Chinese Academy of Sciences, Beijing 100190, People's Republic of China
[4] High Field Laboratory for Superconducting Materials, Institute for Materials Research, Tohoku University, Sendai 980-8577, Japan
[5] Department of Physics, Nanjing University, Nanjing 210093, People's Republic of China

E-mail: ywma@mail.iee.ac.cn

CrossMark

Abstract

The high upper critical field and low anisotropy of iron-based superconductors (IBS) make them particularly attractive for high-field applications, especially for the construction of next-generation nuclear magnetic resonance spectrometers, particle accelerators and high-field magnets. However, for practical use it is essential to make IBS materials into wire and tape conductors with sufficient current carrying capability, which is limited by misaligned grains inside the conductors. Here, based on a simple and low-cost powder-in-tube (PIT) method, we demonstrate a high transport critical current density (J_c) reaching 1.5×10^5 A cm^{-2} ($I_c = 437$ A) at 4.2 K and 10 T in Ba$_{0.6}$K$_{0.4}$Fe$_2$As$_2$ (Ba-122) tapes by texturing the grain orientation with optimized hot-press technique. The transport J_c measured at 4.2 K under high magnetic fields of 27 T is still on the level of 5.5×10^4 A cm^{-2}. Moreover, at 20 K and 5 T the transport J_c is also as high as 5.4×10^4 A cm^{-2}, showing a promising application potential in moderate temperature range which can be reached by liquid hydrogen or cryogenic cooling. All these J_c values are the highest ever reported for IBS wires and tapes. The high-performance PIT Ba-122 tapes in this work suggest IBS to be a strong potential competitor of cuprate superconductors for the race of high-field applications in the future.

Keywords: critical current density, powder-in-tube method, iron-based superconducting tapes

(Some figures may appear in colour only in the online journal)

Introduction

Since the discovery of iron-based superconductors (IBS) in 2008 [1–6], many researchers have engaged in exploring their superconducting mechanism and practical applications [7]. Among them, 122-type IBS are quite attractive for applications since they have a relatively high transition temperature T_c (~38 K) [3], a high upper critical field H_{c2} (>100 T) [8, 9], superior transport J_c (~10^6 A cm^{-2}) in films and very small H_{c2}^{ab}/H_{c2}^{c} anisotropy (1.5–2) [10, 11]. Although the cuprate

superconductors hold very high J_c value, the obstacles such as the extremely high anisotropies and weak link behavior at grain boundary limit their applications. In addition, the brittle texture property in cuprate superconductor, such as YBCO, imposes a restriction on its fabrication and increases the manufacturing costs. For IBS, the inter-grain critical current density J_c^{gb} decrease rapidly when the misalignment of crystalline orientation angles at grain boundaries are larger than 9° [12] and this value is larger than that in YBCO [13]. Currently, the Nb$_3$Sn, a low T_c superconductor is still adopted

1

to generate high field at 4.2 K. However, the sensitivity to strain in Nb_3Sn makes this type of superconductor need a post-winding heat treatment and this process increased the complexity in fabricating wires. We recommend that the IBS may be a more competitive candidate in the competition of superconductors for high-field applications.

Significant researches have been undertaken to fabricate IBS wires and tapes, among which the powder-in-tube (PIT) method is widely adopted [14]. However, the poor connectivity and weak link behavior between grains severely limit the current flow. In the past several years, various strategies were proposed to overcome these obstacles such as metal additions [15], flat rolling [16, 17], uniaxial pressing [18, 19], and hot isostatic pressing [20, 21]. These methods are effective in increasing the connectivity of grains and *c*-axis texture. For example, Sn-doped superconducting powder can enhance the crystallization of grains during the heat treatment [22]. The mechanical deformation in the PIT process can significantly enhance the superconducting core density and the uniaxial rolling and press can induce *c*-axis texture. In addition, reducing voids and inducing oriented *c*-axis texture, which is crucial to relieve the problem of weak link behavior are the key points to further improve the J_c performance.

Previous works in fabricating tapes with hot-pressing (HP) process are usually using $Sr_{0.6}K_{0.4}Fe_2As_2$ (Sr-122) materials. The *c*-axis texture of the rolled Sr-122 superconducting tapes can be significantly increased by the HP process. The transition temperature of Ba-122 rolled tapes is higher than that of the Sr-122 rolled tapes [16, 23]. In this work, high-performance $Ba_{0.6}K_{0.4}Fe_2As_2$ superconducting tapes were successfully fabricated by optimized HP process for the first time. The transport J_c at 4.2 K reaches $1.5 \times 10^5 \, A \, cm^{-2}$ (10 T) and $5.5 \times 10^4 \, A \, cm^{-2}$ (27 T), respectively, and these J_c values are the highest values in IBS wires and tapes ever reported. The *c*-axis texture degree for the HP Ba-122 tapes was found to be higher than that of the flat-rolled Ba-122 tapes and the HP Sr-122 tapes [16, 24]. With these results, we recommend that the Ba-122 materials are flexible to build textured microstructure and the highly textured Ba-122 tapes are beneficial to improve the transport property.

Experimental details

The precursor of Ba-122 was prepared by a solid-state reaction method and the tape was prepared by the *ex situ* PIT process with Sn (5%) as additive. Ba fillings (99%), K pieces (99.95%), As (99.95%) and Fe (99.99%) powders with a nominal composition of $Ba_{0.6}K_{0.5}Fe_2As_2$ were loaded into Nb tube after ball-milling for 10 h under argon atmosphere. Then the tube was heat-treated at 900 °C for 35 h. The sintered precursor was ground into powder, mixed with Sn material in an agate mortar and finally packed into Ag tube (outer diameter: 8 mm and inner diameter: 5 mm). Then the Ag tube with mono-core inside was swaged and drawn into a wire with diameter of 1.9 mm and flat rolled into tapes with thickness of 0.3 mm. The HP process was adopted to the

rolled tapes with a pressure about 15 MPa at 880 °C for 1 h and the thickness of final tapes is 0.25 mm.

The transport critical current I_c was measured by the standard four-probe method with a criterion of $1 \, \mu V \, cm^{-1}$ under 4.2 K at the High Field Laboratory for Superconducting Materials at Sendai. We carried out I_c measurement by using a superconducting magnet and a hybrid magnet up to 14 T and 27 T, respectively. The transport I_c values with different field directions are measured by soldering the samples on a sample holder which can be rotated. The samples were measured with a sequence of tape surface vertical, a 45° and parallel to the field directions. The phase construction of superconducting cores was measured by x-ray diffraction (XRD) using Bruker D8 Advance diffractometer with Cu Kα radiation after peeling off the Ag sheathe. The electromagnetic properties were measured on Physical Property Measurement System (Quantum Design). In order to investigate the vortex pinning mechanism of our tape, we used the Dew-Hughes model [25] and the magnetization property of superconducting core was measured by SQUID-VSM on Magnetic Property Measurement System (Quantum Design). The samples were inlay into the epoxy resin and the tape surfaces were polished well with SiO_2 papers and SiO_2 suspension. In order to eliminate the stress of the tape surface which produced during the polishing process, the vibratory polisher (VibroMet 2, Buehler) was adopted. The crystal orientation was analyzed by electron backscatter diffraction (EBSD) plugin equipped on scanning electron microscope (Zeiss SIGMA). The superconducting cores are taken from the tapes with peeling off the silver sheath and pasted on a platform with the normal direction vertical to the platform surface. The samples were polished by polished papers with different mesh until the sample surface is smooth enough, then we melted down the samples and polish the other side of the samples. The thickness of measurement area is less than 100 nm. The TEM measurement were adopted on a JEOL JEM-2100F TEM.

Results and discussion

Figure 1 shows the magnetic field dependence of the transport critical current density J_c at 4.2 K of Ba-122 tapes and the properties of other type of superconducting wires or tapes are also included [26–29]. The transport J_c at 4.2 K in this work reaches $1.5 \times 10^5 \, A \, cm^{-2}$ ($I_c = 437 \, A$) at 10 T and $5.5 \times 10^4 \, A \, cm^{-2}$ at 27 T, respectively. These J_c values are the highest values ever reported for all of the IBS wires and tapes. The extrapolated J_c curves of the two batches of samples intersect with the J_c curve of Nb_3Sn around the field of 18 T, indicating that the IBS is a competitive candidate for high-field applications. In addition, the engineering critical current density (J_e) of the samples achieves $3 \times 10^4 \, A \, cm^{-2}$ at 4.2 K and 10 T. This value is higher than that of the flat-rolled Ba-122 tapes and the HP Sr-122 tapes [30]. We also calculated the *n*-values to evaluate the uniformity and stability of the HP samples. The *n*-value of HP tapes at 10 T is 65.2
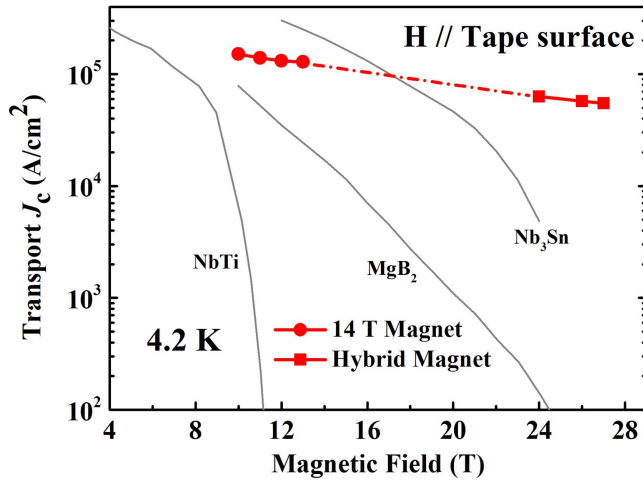
Figure 1. Magnetic field dependence of transport critical current density J_c for the hot-pressed Ba-122 tape at 4.2 K. The transport J_c of other wires or tapes are also included for comparison.
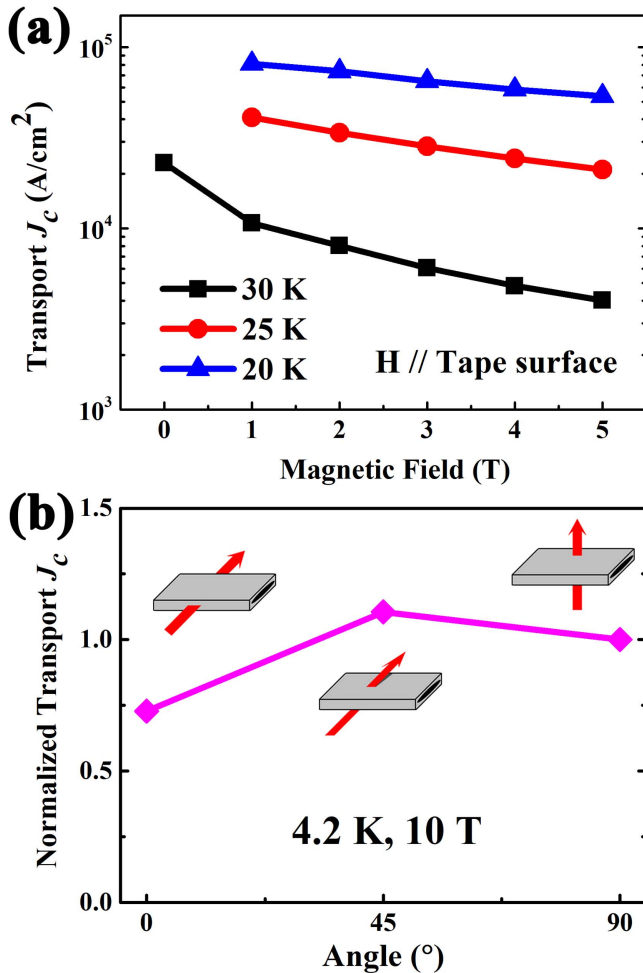

Figure 2. Magnetic field dependence of transport critical current density J_c at various temperatures and in various field directions. (a) The magnetic field dependence of transport J_c for the hot-pressed Ba-122 tape at 30 K, 25 K and 20 K, respectively. (b) The normalized transport J_c measured at 4.2 K, 10 T with the direction of magnetic field parallel, vertical and a 45° to the tape surface, respectively.

which is much higher than that of the rolled Sr-122 tapes and the 7-filament tapes [31, 32], indicating a good homogeneity of the Ba-122 superconducting core. Figure 2(a) shows the magnetic field dependence of J_c for the HP Ba-122 tape at 30 K, 25 K and 20 K, respectively. The J_c values remain 5.4×10^4 A cm^{-2} at 5 T when the temperature rises to 20 K and these values are also the highest at such fields and temperatures. These results indicate the potential applications of IBS in medium temperature range which can be reached by liquid hydrogen or cryogenic cooling. As shown in figure 2(b), we also measured the transport J_c with the tape surface parallel, vertical and an angle of 45° to the direction of magnetic field, respectively. The J_c (4.2 K, 10 T) are normalized by the value measured at 90° i.e., tape surface vertical to the field direction, to show the J_c anisotropy of Ba-122 superconducting tapes. It can be seen clearly that the J_c values measured with the tape surface vertical to the field direction are higher than that of parallel to the field direction, which is different from the cuprate superconductors. The unusual anisotropic behaviors may be originated by the strong random pinning center which is larger than the coherence length and this phenomenon also can be found in the HP Sr-122 superconducting tapes [33]. The J_c anisotropy of the HP Ba-122 tape at 10 T is 1.37, and this value is much smaller than that of the Bi-2223 and YBCO tapes. These results demonstrate a nearly isotropic behavior of transport J_c under magnetic fields in different directions, suggesting that the IBS are beneficial to manufacture superconducting magnets.

The electromagnetic properties of the superconducting core were examined. Figure 3(a) shows the curves of the resistivity as a function of temperature and figure 3(b) exhibits the details. The T_c^{onset} and T_c^{zero} are 37.6 K and 37.3 K at 0 T, respectively. The resistivity transition width $\Delta T_c = 0.3$ K is sharper than that of the Sr-122 tapes by HP process [18] and this result demonstrates that the electromagnetic properties of the tape are homogeneous. The magnetization as a function of temperature for the HP tape was measured with a 20 Oe magnetic field parallel to the tape surface as shown in figure 3(c). The rather sharp superconducting transition indicates high quality superconducting phases and nearly the whole bulk of superconducting core we measured exhibits superconductivity property. Furthermore, the FC curve is independent of temperature indicating strong vortex pinning in the tape.

XRD patterns of the superconducting core of HP tape are shown in figure 3(d) and the data of precursor powder is also included for comparison. A well-defined ThCr$_2$Si$_2$-type crystal structure can be found from the XRD patterns and the Ag peaks are also indexed because of the Ag sheath. Obviously, the (00*l*) peaks were strongly enhanced by the cold-work deformation and the HP process when comparing the peaks between the superconducting core and the randomly oriented precursor. The degree of *c*-axis texture can be calculated by the Lotgering method [34] with $F = (\rho - \rho_0)/(1 - \rho_0)$, where $\rho = \Sigma I(00l)/\Sigma I(hkl)$, $\rho_0 = \Sigma I_0(00l)/\Sigma I_0(hkl)$. I and I_0 are the intensities of each peak for the textured and randomly oriented samples, respectively. The F value is 0.87 which is higher than that of the HP Sr-122 tapes and the cold-pressed Ba-122 tapes [24, 35]. These results indicate that the crystal orientations of Ba-122 are
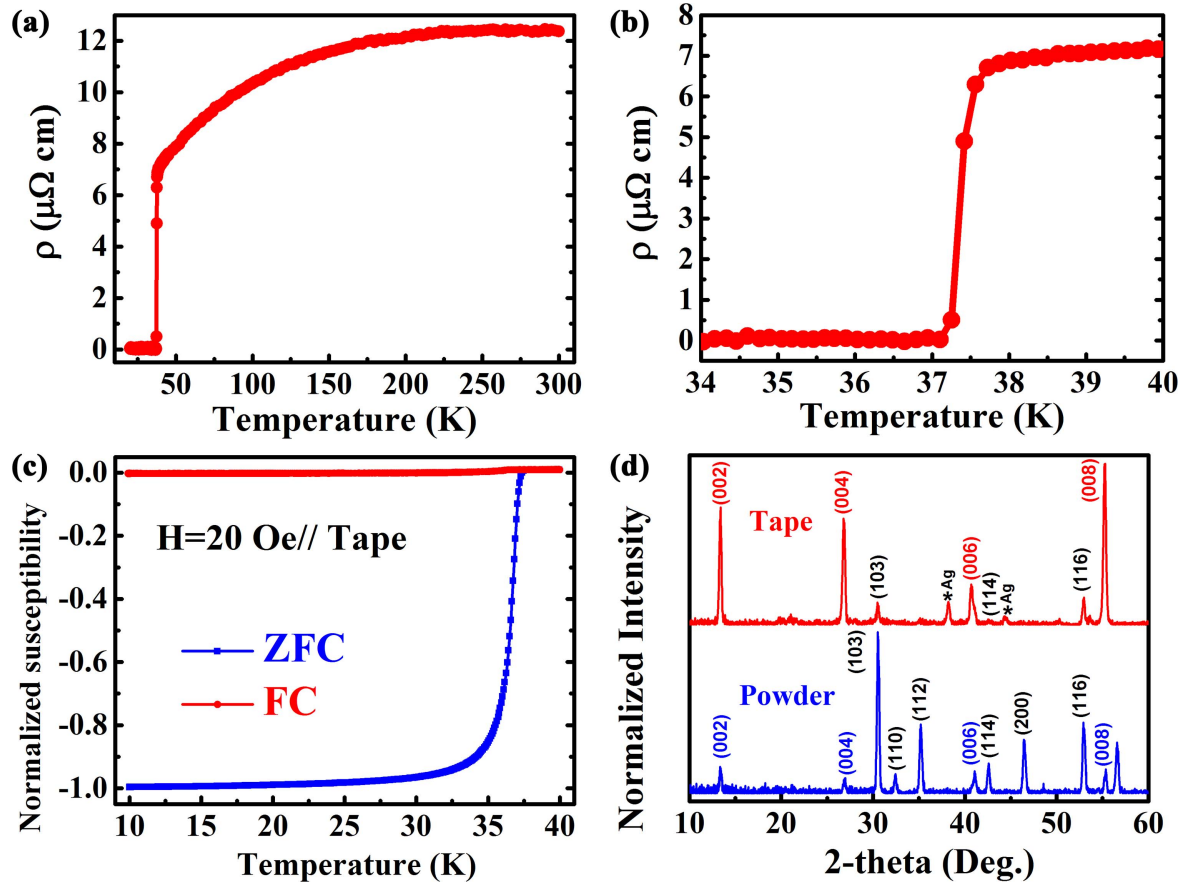
Figure 3. Electromagnetic properties and crystal microstructure of the superconducting core of hot-pressed tape. (a) and (b) The resistivity as a function of temperature. (c) Temperature dependence of the susceptibility for the superconducting core with zero field cooling (ZFC) and field cooling (FC) procedures. (d) XRD patterns for the superconducting core of the HP tape. The data of randomly orientated powder is also included as a reference.

prone to rotate along the tape surface by the pressure which applied to the tape surface and thus the *c*-axis texture was enhanced. In addition, the core density is another important parameter which relates to the transport J_c and sometimes shows a positive relation with the transport J_c [35]. However, the average Vickers hardness value of the superconducting core of the HP tape is 138, higher than that of the flat-rolled tape but lower than that of the stainless steel sheathed cold-pressed tapes (~200) [16, 35]. It is obvious that the core density of Ba-122 tapes were enhanced by the HP process, but the materials of the silver sheath restrict the further enhancement of the superconducting core density. Comparing the texture and core density of the tapes which fabricated by cold-pressing method with our results, we hold that the texture may a dominant parameter which influence the transport J_c of Ba-122 tapes in this work.

The EBSD technique is an important tool to thoroughly characterize the microstructure, grain size and crystal orientation of the superconducting core [36]. The grain orientation and the misorientation angle between grains can be marked by the automatic detected Kikuchi patterns after polishing the center section of superconducting core well. Figure 4(a) shows the grain size with the neighboring grains marked with different colors in order to identify the different grains. Most

grains with the diameter lower than 2 μm are evenly constructed parallel to the tape surface. The grain size of the HP Ba-122 superconducting tape is smaller than that of the HP Sr-122 tape [24]. In order to quantitatively describe the grain size properties, we plot grain numbers and areas as functions of grain size diameter, which is shown in the inset of figure 5. The grain size diameter is defined as $D = 2(A/\pi)^{1/2}$, where A is the area of detected grains. Most grains with diameter of 0.5–1 μm are detected from the EBSD image and this diameter is much smaller than that of HP Sr-122 tapes and the flat-rolled Ba-122 tapes. As we know, in a specific area, the more grains with small size usually means the larger grain boundaries density. Here, the grains with diameter between 1 and 2.5 μm occupy the main area indicating a homogeneous grain size in the superconducting core.

It is found that grain boundary pinning is dominant in the vortex pinning mechanism in HP Sr-122 superconducting tapes [37]. We plot the $J_c^{mag1/2} \times \mu_0 H^{1/4}$ as a function of $\mu_0 H$ to calculate the irreversibility field H_{irr} as shown in the inset of figure 6 where J_c^{mag} is the magnetic critical current density. The J_c^{mag} is obtained from the isothermal hysteresis loops based on the Bean model [38]. We estimate the H_{irr} value by linear fitting the curves to zero $J_c^{1/2} \times \mu_0 H^{1/4}$ value
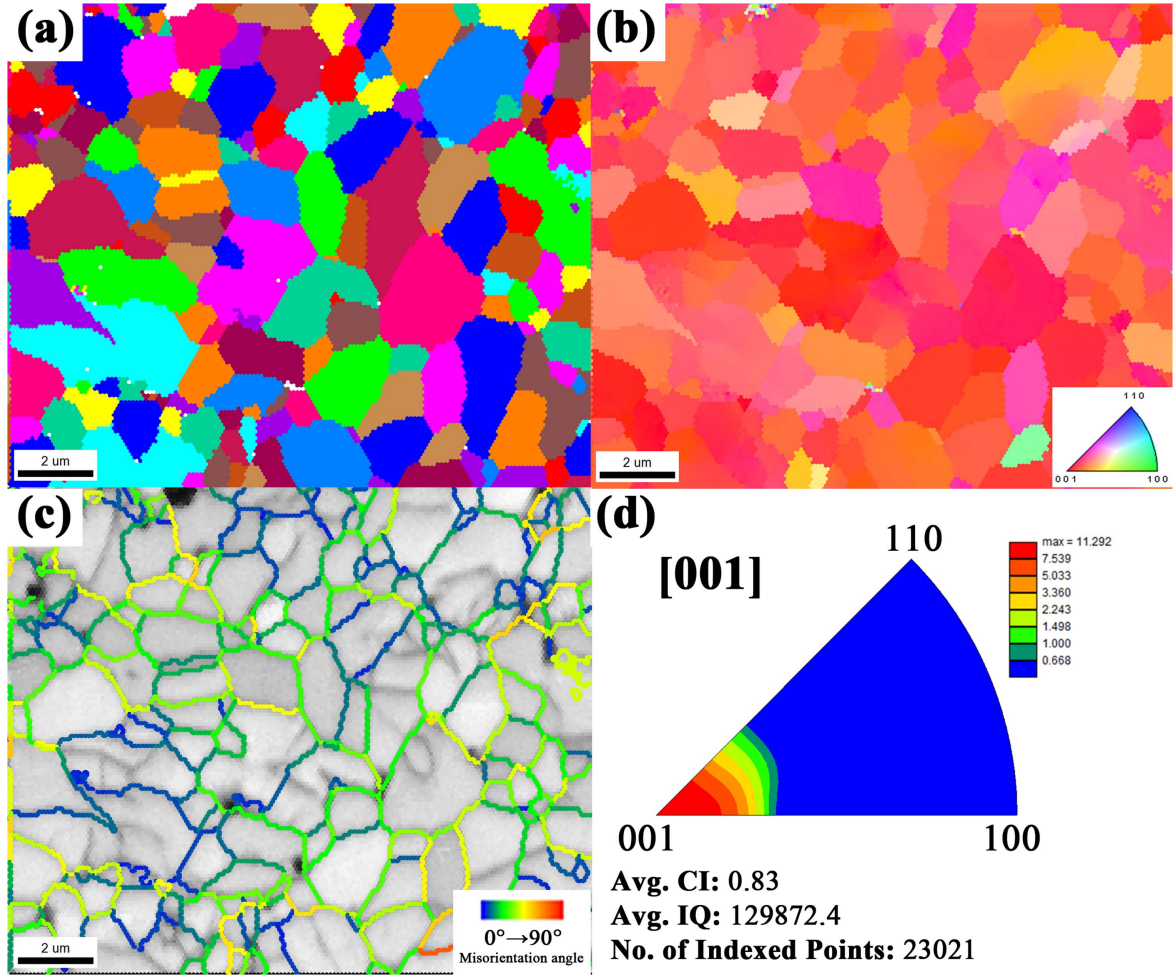
Figure 4. EBSD images for the superconducting core of the HP tape viewed from the ND direction of the tape. (a) The marked neighboring grains with different colors. (b) The inverse pole figure (IPF) image in [001] direction. (c) The misorientation angle loaded to the grain boundaries. The color codes of this image are posted out on the bottom right corner of this image. (d) The inverse pole figure in [001] direction for the measured area.
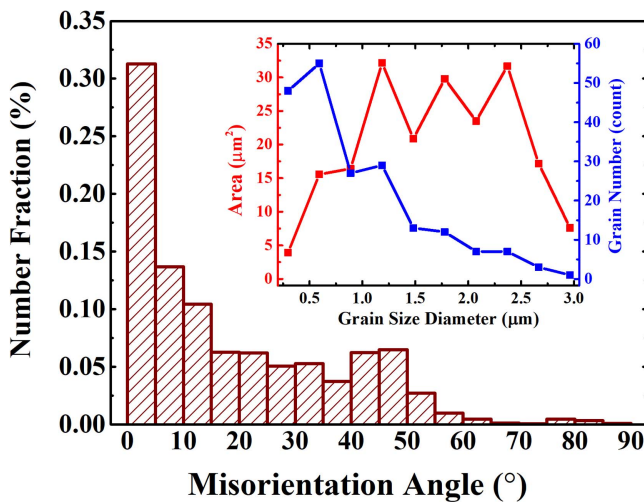
Figure 5. Misorientation angle distribution for the superconducting core of the HP tape. The inset shows the grain size distribution compared with the grain number (blue line) and the area (red line), respectively.
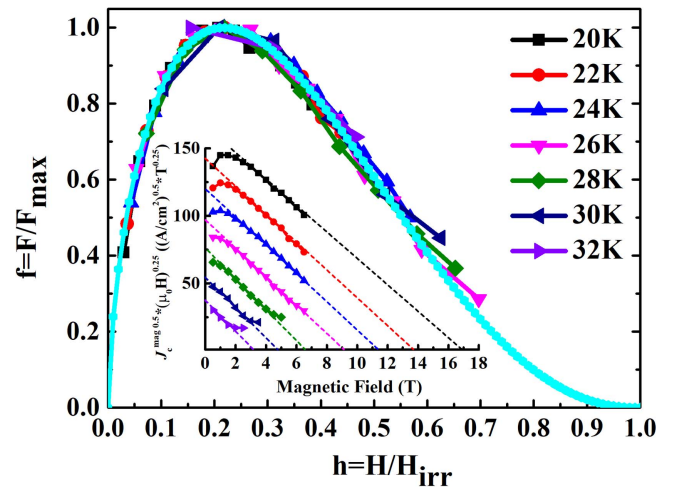
Figure 6. Normalized vortex pinning force $f = F_p/F_p^{max}$ as a function of the reduced field $h = H/H_{irr}$. The fitting curve using the formula $f = Ah^p(1 - h)^q$ with cyan color is also included. The inset shows the Kramer plot for 22–32 K with a step length 2 K per curve. The curves are linear fitted with dash line.
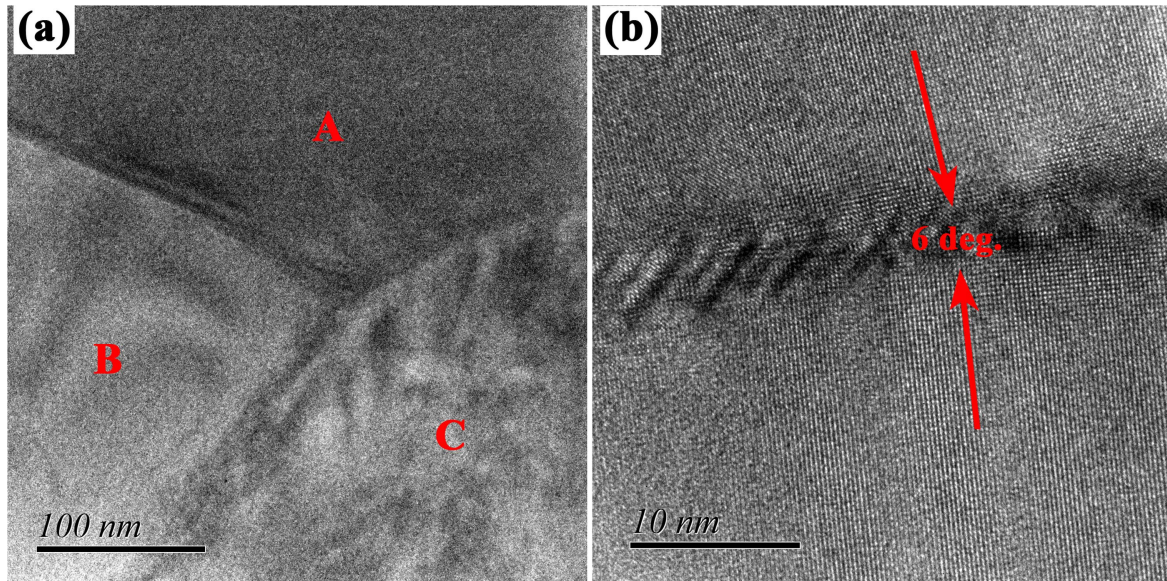
Figure 7. The TEM image of the superconducting core. (a) The clean and well-connected grain boundaries. (b) A random grain boundary with small misorientation angle.

[39]. According to the Dew-Hughes model [25], if a dominant pinning mechanism exists in the superconducting tape, a unified function $f = Ah^p(1 - h)^q$ can be used at different temperature where f is the normalized vortex pinning forces and A is a constant. The results are shown in figure 6 in which the curves of $f(h, T)$ at different temperature show the same trend and almost overlap with each other. This result demonstrate that the pinning mechanism is independent of temperature and the function $f = Ah^p(1-h)^q$ can be used in this situation. The cyan color curve in figure 6 is fitted to the $f(h, T)$ curves at different temperature with $p = 0.64$ and $q = 2.3$. We can calculate the peak position by $h_{max} = p/(p + q) = 0.22$ which is the same with the observed h_{max} value from fitted curve. The h_{max} value is close to 0.2 and according to the Dew-Hughes model, the pinning mechanism of the HP tape belongs to surface pinning [37]. We recommend that the grain boundary pinning is dominant in our tape which is same with the HP Sr-122, Nb_3Sn and MgB_2 superconducting wires and tapes [40, 41]. The relative small grain size is beneficial to the improvement of the vortex pinning property. This phenomenon also can be found in MgB_2 superconductors where the pinning force increases with the decreasing grain size when the sample with good grain connectivity [42].

Figure 4(b) shows the inverse pole figure (IPF) map which is given in [001] direction with the color code drawn in the stereographic triangle. The red color reveals that the dominant orientation of grains is (001), indicating the strong c-axis texture and it is also confirmed by the IPF figure shown in figure 4(d). These results clarify that the c-axis of almost all of the Ba-122 grains are perpendicular to the tape surface. Figure 4(c) directly shows the misorientation angle loaded to the grain boundaries. The blue and green color indicate that the misorientation angles between grains at low angle hold a considerable proportion which can be indexed from the color code. We also list the quantified number fraction diagrams of

the determined misorientation angle in the range of 1°–90° which is shown in figure 5. It clarifies that the number fraction, which represents the grain boundary length, decreases with increasing the misorientation angle. We also give the quantitative description about the grain boundaries of the measured area and there are 42.8% of number fractions within 9° which is higher than that of the Sr-122 superconducting tape [24]. In addition, the average confidence index, the average image quality and the number of indexed good points are also included in the bottom of figure 4(d) indicating the EBSD results are reliable enough.

The TEM technology is adopted to further investigate the microstructure of the grain boundaries. Figure 7 gives a typical TEM image from the plan view of the tape. Figure 7(a) shows three grains marked with A, B and C and the grain boundaries are clean and well-connected. Figure 7(b) is a typical grain boundary with a misorientation angle 6° and many grain boundaries with low misorientation angle can be found from the superconducting core which is confirmed by the results of EBSD. Combining the data of TEM and EBSD, we recommend that the rolling deformation in the PIT process and the force applied to the tape during the heat treatment can effectively enhance the grain connectivity and improve the c-axis texture.

In the PIT process, the c-axis texture produced during the rolling deformation as well as the residual microcracks. However, the HP process makes these microcracks more flexible to couple with each other and thus inhibit the crumple of grains and continue to improve the c-axis texture. This result is also confirmed by the IPF figures from EBSD. In addition, a large amount of grain boundaries with low angle are detected by the TEM which indicating that the weak-link behavior is suppressed in our tape. Therefore, the strong degree of c-axis texture and the improved connectivity between grains are the reasons to the high J_c values.

Conclusion

In this work, we systematically studied the properties of the high-performance Ba-122 superconducting tapes fabricated by HP process. The transport J_c values achieve 1.5×10^5 A cm^{-2} ($I_c = 437$ A) at 10 T and 5.5×10^4 A cm^{-2} at 27 T, respectively. In addition, the transport J_c achieves as high as 5.4×10^4 A cm^{-2} at 5 T and 20 K. This is the first report in Ba-122 tapes with such high transport J_c values. These J_c values are the highest ever reported in IBS wires and tapes and are also superior to NbTi, Nb$_3$Sn and MgB$_2$ tapes or wires. We find a high degree c-axis texture in the Ba-122 tapes and a large number of grain boundaries within $9°$ are detected. These J_c results further strengthen the position of IBS as a competitor to other superconductors in high field applications.

Acknowledgments

ORCID iDs

He Huang ⬤ https://orcid.org/0000-0002-8482-3682

References

[1] Kamihara Y, Watanabe T, Hirano M and Hosono H 2008 *J. Am. Chem. Soc.* **130** 3296
[2] Ren Z A *et al* 2008 *Chin. Phys. Lett.* **25** 2215
[3] Rotter M, Tegel M and Johrendt D 2008 *Phys. Rev. Lett.* **101** 107006
[4] Hsu F C *et al* 2008 *Proc. Natl Acad. Sci.* **105** 14262
[5] Wang X C, Liu Q Q, Lv Y X, Gao W B, Yang L X, Yu R C, Li F Y and Jin C Q 2008 *Solid State Commun.* **148** 538
[6] Sasmal K, Lv B, Lorenz B, Guloy A M, Chen F, Xue Y Y and Chu C W 2008 *Phys. Rev. Lett.* **101** 107007
[7] Putti M *et al* 2010 *Supercond. Sci. Technol.* **23** 034003
[8] Altarawneh M M, Collar K, Mielke C H, Ni N, Bud'ko S L and Canfield P C 2008 *Phys. Rev.* B **78** 220505
[9] Gurevich A 2011 *Nat. Mater.* **10** 255
[10] Yuan H Q, Singleton J, Balakirev F F, Baily S A, Chen G F, Luo J L and Wang N L 2009 *Nature* **457** 565
[11] Yamamoto A *et al* 2008 *Appl. Phys. Lett.* **92** 252501
[12] Katase T, Ishimaru Y, Tsukamoto A, Hiramatsu H, Kamiya T, Tanabe K and Hosono H 2011 *Nat. Commun.* **2** 409
[13] Dimos D, Chaudhari P and Mannhart J 1990 *Phys. Rev.* B **41** 4038
[14] Ma Y 2012 *Supercond. Sci. Technol.* **25** 113001
[15] Wang L, Qi Y, Gao Z, Wang D, Zhang X and Ma Y 2010 *Supercond. Sci. Technol.* **23** 025027
[16] Dong C H, Yao C, Lin H, Zhang X P, Zhang Q J, Wang D L, Ma Y W, Oguro H, Awaji S and Watanabe K 2015 *Scr. Mater.* **99** 33
[17] Huang H, Zhang X, Yao C, Dong C, Zhang Q, Ma Y, Oguro H, Awaji S and Watanabe K 2016 *Physica* C **525–526** 94
[18] Zhang X *et al* 2014 *Appl. Phys. Lett.* **104** 202601
[19] Togano K, Gao Z, Taira H, Ishida S, Kihou K, Iyo A, Eisaki H, Matsumoto A and Kumakura H 2013 *Supercond. Sci. Technol.* **26** 065003
[20] Pyon S, Yamasaki Y, Kajitani H, Koizumi N, Tsuchiya Y, Awaji S, Watanabe K and Tamegai T 2015 *Supercond. Sci. Technol.* **28** 125014
[21] Weiss J D, Tarantini C, Jiang J, Kametani F, Polyanskii A A, Larbalestier D C and Hellstrom E E 2012 *Nat. Mater.* **11** 682
[22] Lin H, Yao C, Zhang X P, Zhang H T, Wang D L, Zhang Q J and Ma Y W 2013 *Physica* C **495** 48
[23] Wang L, Qi Y, Wang D, Zhang X, Gao Z, Zhang Z, Ma Y, Awaji S, Nishijima G and Watanabe K 2010 *Physica* C **470** 183
[24] Lin H *et al* 2014 *Sci. Rep.* **4** 6944
[25] Dew-Hughes D 2006 *Phil. Mag.* **30** 293
[26] Ye S and Kumakura H 2016 *Supercond. Sci. Technol.* **29** 113004
[27] Parrell J A, Youzhu Z, Field M B, Cisek P and Seung H 2003 *IEEE Trans. Appl. Supercond.* **13** 3470
[28] Boutboul T, Le Naour S, Leroy D, Oberli L and Previtali V 2006 *IEEE Trans. Appl. Supercond.* **16** 1184
[29] Kanithi H, Blasiak D, Lajewski J, Berriaud C, Vedrine P and Gilgrass G 2014 *IEEE Trans. Appl. Supercond.* **24** 1
[30] Ma Y 2015 *Physica* C **516** 17
[31] Yao C, Wang D, Huang H, Dong C, Zhang X, Ma Y and Awaji S 2017 *Supercond. Sci. Technol.* **30** 075010
[32] Liu F *et al* 2017 *Supercond. Sci. Technol.* **30** 07LT01
[33] Awaji S, Nakazawa Y, Oguro H, Tsuchiya Y, Watanabe K, Shimada Y, Lin H, Yao C, Zhang X and Ma Y 2017 *Supercond. Sci. Technol.* **30** 035018
[34] Lotgering F K 1959 *J. Inorg. Nucl. Chem.* **9** 113
[35] Gao Z, Togano K, Matsumoto A and Kumakura H 2015 *Supercond. Sci. Technol.* **28** 012001
[36] Koblischka-Veneva A, Koblischka M R, Schmauch J, Inoue K, Muralidhar M, Berger K and Noudem J 2016 *Supercond. Sci. Technol.* **29** 044007
[37] Dong C, Lin H, Huang H, Yao C, Zhang X, Wang D, Zhang Q, Ma Y, Awaji S and Watanabe K 2016 *J. Appl. Phys.* **119** 143906
[38] Bean C P 1964 *Rev. Mod. Phys.* **36** 31
[39] Kramer E J 1973 *J. Appl. Phys.* **44** 1360
[40] Larbalestier D, Gurevich A, Feldmann D M and Polyanskii A 2001 *Nature* **414** 368
[41] Kroeger D M, Easton D S, DasGupta A, Koch C C and Scarbrough J O 1980 *J. Appl. Phys.* **51** 2184
[42] Martínez E, Mikheenko P, Martínez-López M, Millán A, Bevan A and Abell J S 2007 *Phys. Rev.* B **75** 134515